Correlation Between Microstructure and Ageing of Iron Manganite Thermistors

T. Battault, R. Legros, M. Brieu, J. Coudere, L. Bernard, A. Rousset

Correlation Between Microstructure and Ageing of Iron Manganite Thermistors

T. Battault ([1]), R. Legros ([1]), M. Brieu ([1]), J.J. Couderc ([2]), L. Bernard ([2]) and A. Rousset ([1,*])

([1]) Laboratoire de Chimie des Matériaux Inorganiques ([**]), Université Paul Sabatier, 118 route de Narbonne, 31062 Toulouse Cedex, France.

([2]) Laboratoire de Physique des Solides ([***]), INSA, Complexe Scientifique de Rangueil, 31077 Toulouse Cedex, France

(Received 26 June 1996, revised 21 November 1996, accepted 31 January 1997)

PACS.81.40.Rs – Electrical and magnetic properties (related to treatment conditions)
PACS.61.16.Bg – Transmission, reflection and scanning electron microscopy (including EBIC)
PACS.61.72 Mm – Grain and twin boundaries

Abstract. — Negative Temperature Coefficient (NTC) thermistors made of spinel structure transition metal manganites usually display ageing phenomena under thermal stress. Their resistance drift depends on their composition, crystal structure (cubic or tetragonal) and heat treatments We have previously shown in iron manganite thermistors, $Mn_{3-x}Fe_xO_4$ (with $0 \leq x \leq 1.51$), that the ageing is due to the migration of Fe^{3+} and Mn^{2+} ions between tetrahedral and octahedral sites of the spinel structure. Iron manganites were investigated by Transmission Electron Microscopy (TEM) in order to relate microstructure to electrical stability For iron manganites with iron content $x \leq 0.78$, two dimensional defects result in a domain microstructure (microtwins). As x increases and exceeds 0.78, the domain structure gradually vanishes and transforms into a tweed microstructure ($x = 1.05$) and, for $x > 1.30$, no bidimensional defects are observed. Thus it is suggested that the microstructural disturbance plays an important role in the kinetics of the ion migration during the ageing of the studied ceramics.

Résumé. — Les thermistances à Coefficient de Température Négatif (CTN) élaborées à partir de manganites de métaux de transition à structure spinelle présentent, sous contrainte thermique, le phénomène de vieillissement. La dérive de leur résistance dépend de la composition chimique, de la structure cristallographique (cubique ou quadratique) et des traitements thermiques Précédemment, nous avons montré, pour les thermistances à base de manganites de fer de composition $Mn_{3-x}Fe_xO_4$ (avec $0 \leq x \leq 1,51$), que le vieillissement est dû à une migration des ions Fe^{3+} et Mn^{2+} entre les sites tétraédriques et octaédriques de la structure spinelle. Une étude des manganites de fer a été réalisée par Microscopie Électronique à Transmission (MET) afin de relier la microstructure à la stabilité électrique. Pour les manganites de fer ayant une teneur en fer $x \leq 0,78$, la microstructure en forme de domaines (micromaclages) résulte de la présence de deux types de défauts bidimensionnels Pour des teneurs supérieures, jusqu'à 0,78, cette microstructure disparaît graduellement et se transforme en une microstructure tweed

(*) Author for correspondence (e-mail rousset@iris.ups-tlse fr)
(**) CNRS ESA 5070
(***) CNRS ERS 111

($x = 1,05$) et, pour $x > 1,30$, aucun défaut bidimensionnel n'est observé Ces observations nous ont conduits à suggérer que ces différences dans la microstructure influencent grandement la cinétique de migration des ions durant le vieillissement des céramiques étudiées.

1. Introduction

Transition-metal manganites are technologically important for use in thermally sensitive resistors [1–5]. They have gained extensive use as temperature sensors over a number of years, and are widely used for temperature measurement in air conditioners, refrigerators, medical, and other fields.

The electrical transport phenomena of these materials are frequently interpreted in terms of phonon-assisted jump of carriers among localized states, the so-called hopping conductivity [1, 6]. Unfortunately, Negative Temperature Coefficient (NTC) thermistors made of spinel structure transition metal manganites usually display ageing phenomena under thermal stress: their resistance R increases with time. Their resistance drift $\Delta R/R$ depends on their chemical composition, their crystal structure (cubic or tetragonal), and the heat treatments applied [7,8].

In a previous paper [9] we presented the results of Transmission Electron Microscopy (TEM) characterization of Ni and Ni-Co manganites. These experiments generated new information concerning the microstructure and phase composition of these materials after slow cooling (6 °C/h) or quenching. The improvement in electrical stability might be related to the existence of a "tweed" structure, *i.e.* fine-scaled bidimensional lattice defects parallel to {110}.
Several processes have been proposed to explain the origin of ageing, namely ion oxidation, and ionic and/or electronic migration [8, 10]. The one most commonly retained is migration of cations during various heat treatments. Since ageing is believed to be correlated to atomic diffusion in the spinel lattice, the intergranular defects could act as barriers against ion mobility thus explaining the better thermal stability of quenched ceramic.

In spite of its high resistivity, iron manganites $Mn_{3-x}Fe_xO_4$ have NTC thermistor characteristics [11]. Using Mössbauer results, we have previously shown that the origin of the ageing in these thermistors is due to the migration of Fe^{3+} and Mn^{2+} ions between tetrahedral (A) and octahedral (B) sites of the spinel structure and inverse migration of Mn^{2+} ions [12].

The aim of this paper is to extend TEM characterization to a series of iron manganites $Mn_{3-x}Fe_xO_4$ with iron content $0 \leq x < 1.51$, to determine the role of defects on ion migration during ageing.

2. Experimental

2.1. Preparation of Ceramic Samples. — Thermal decomposition of coprecipitated formate precursors is a direct method for the preparation of pure, homogeneous iron manganite spinel powders [11], and consequently improves measurement reproducibility. The obtained oxide powders were mixed with an organic binder pressed into disks at a pressure of 400 MPa. The green disks were fired at 1180 °C in air and sintered 4 hours, then quenched in air. In this latter treatment, the samples were simply taken out of the furnace (mean cooling rate 300 °C min^{-1}).

A batch of iron manganites were prepared with formula $Mn_{3-x}Fe_xO_4$ and with $0 \leq x \leq 1.51$. The specifications of all samples used in this study are listed in Table I.

Table I. — *Composition of the formate precursors* $Fe_yMn_{1-y}(O_2CH), 2H_2O$ *and the corresponding iron manganites* $Fe_xMn_{3-x}O_4$.

y	0	0.04	0.13	0.19	0.26	0.35	0.43	0.50
x	0	0.12	0.39	0.58	0.78	1.05	1.30	1.51

2.2. MEASUREMENTS. — To determine their electrical characteristics, the ceramic samples were electroded with silver paint on the opposite faces of the sintered discs and an 850 °C heat treatment was performed in a tunnel furnace in order to get a good metal-ceramic contact. Resistivity ρ was measured at (25 ± 0.05) °C using a Philips PM2525 multimeter. Ageing was measured by the relative variation (drift) $\Delta R/R$ of a NTC thermistor held at 125 °C for intervals ranging up to 1000 h. The instant $t = 0$ corresponds to the time where ceramics were submitted, for the first time, to the heat stress at 125 °C. The error was estimated ±0.5%.

X-ray powder and/or ceramic diffraction (XRD) measurements were performed at room temperature using an automatic diffractometer (Siemens D 501). The lattice parameters were calculated from carefully calibrated records, sodium chloride being used as internal standard. The accuracy of this method is estimated as ±0.0005 nm.

The ^{57}Fe Mössbauer spectra were recorded at room temperature with a spectrometer using a 25 m $Ci^{57}Co$ in Rh matrix. Greater detail is given in previous work [11]. The error in the semi-quantitative Mössbauer analysis is very large, estimated about 20%. Nevertheless, these quantitative results have been confirmed by thermogravimetric analysis, a more precise quantitative technology [13].

2.3. PREPARATION OF SAMPLES FOR TEM. — For TEM observations, the samples were cut in thin slices with a wire saw, then mechanically ground to about 100 μm, and thinned by ionic milling. They were observed in a JEOL 200 CX electron microscope (TEM SCAN Service of the University Paul Sabatier, Toulouse), operating at 200 kV.

3. Results

3 1. ELECTRICAL MEASUREMENTS. — Table II shows the variation in dc resistivity, ρ, as a function of iron content x in iron manganite $Mn_{3-x}Fe_xO_4$. The electrical measurements in these manganites were carried out only for iron contents higher to or equal to $x = 0.39$. The dc resistivity of the composition for $x < 0.39$ was too high for measurement For $x \geq 0.39$, the resistivity decreases rapidly up to $x = 0.78$, then more slowly to $x = 1.51$.

Table II indicates also the various values of ageing, $\Delta R/R$, expressed as a percentage, obtained on iron manganites maintained at 125 °C for 24, 100, 500 and 1000 hours. All monophase ceramics synthesized in this study exhibit resistance drift with time that reaches high values of up to 17% at 1000 hours. Ageing also increases with iron content.

3.2. XRD ANALYSIS. — All $Mn_{3-x}Fe_xO_4$ ($0 \leq x \leq 1.05$) solid solutions crystallize with a spinel structure. Table III gives the overall results, the variation in the lattice parameters a and c, and the ratio c/a. For $0 \leq x < 1.05$, XRD powders revealed a single tetragonally distorted cubic symmetry spinel phase. This tetragonal distortion, characterized by the ratio c/a, decreases with increasing the iron content, x, and disappears for $x = 1.05$.

For $1.05 \leq x \leq 1.51$, iron manganites crystallize with a cubic single phase. The same results were observed on the quenched ceramics and after ageing.

Table II. — *Electrical characteristics of iron manganites: resistivity ρ and ageing $\Delta R/R$ at 125 °C.*

Iron content, x		0.39	0.58	0.78	1.05	1 30	1.51
ρ (Ωcm)		1.43×10^7	9.88×10^6	2.44×10^6	$2\ 02 \times 10^6$	1.80×10^6	1.60×10^6
$\Delta R/R$ (%)	24 h	3.3	3.2	3.1	2.2	9 1	11.0
	100 h	5.4	5.8	4 8	6.4	11 6	11.9
	500 h	7.2	6.4	10 9	13.4	13 8	13.3
	1000 h	10.0	10.4	14 0	15.0	15 4	17.0

Table III. — *Lattice parameters and c/a ratio as a function of iron content, x, for the iron manganite powders.*

Iron content, x	0	0.12	0.39	0.58	0.78	1.05	1.30	1.51
a (nm)	0.8141	0.8192	0.8225	0.8259	0.8274	0.8392	0.8486	0.8501
c (nm)	0.9456	0.9400	0.9300	0.9181	0.9019			
c/a	1.16	1.14	1.13	1.11	1.09	1	1	1

3.3. MÖSSBAUER SPECTROSCOPY. — Mössbauer spectroscopy was carried out on two iron manganites with two different crystallographic structures before ($t = 0$), after 1000 hours ageing ($t = 1000$ h): tetragonal, for $x = 0.58$, and cubic, for $x = 1.05$. All the Mössbauer spectra of these four iron manganites have the same shape. They all exhibit two doublets indicating the presence of two non-equivalent sites of the Fe^{3+} ions in octahedral and tetrahedral sites of the spinel structure. From quantitative analysis [14] we computed the percentage of Fe^{3+} ions in each site. Thus knowing the total number of iron ions in the iron manganite (here 0.58 and 1.05), we calculated the number of Fe^{3+} ions in both sites. All the results are reported in Table IV. Considering the large error of about 20% in the semi-quantitative Mössbauer results, the value of Fe^{3+} ions in tetrahedral sites — 0.29 and 0.23 for $x = 0.58$ and 1.05 respectively — must be assumed to be the same. After calculating the cationic distributions, we shall consider the mean values.

3.4. TEM RESULTS. — The observations were performed on quenched ceramics. Electron diffraction confirms the XRD results concerning the crystal structure of the samples, *i.e.* they are tetragonal (space group $I4_1/amd$) for $x < 1.05$ and cubic spinel (space group Fd3m) for

Table IV. — *Number of Fe^{3+} ions in each site of the spinel structure for the iron manganites $Fe_{0\ 58}Mn_{2\ 42}O_4$ and $Fe_{1\ 05}Mn_{1\ 95}O_4$ at $t = 0$ and $t = 1000$ hours.*

	Octahedral sites		Tetrahedral sites		
Samples	I	II	I	II	mean value
$t = 0$	0.29	0.82	0.29	0.23	0.26
$t = 1000$ h	0.52	0.96	0.06	0.09	0.08

Iron content of the samples I = 0.58 and II = 1.05.

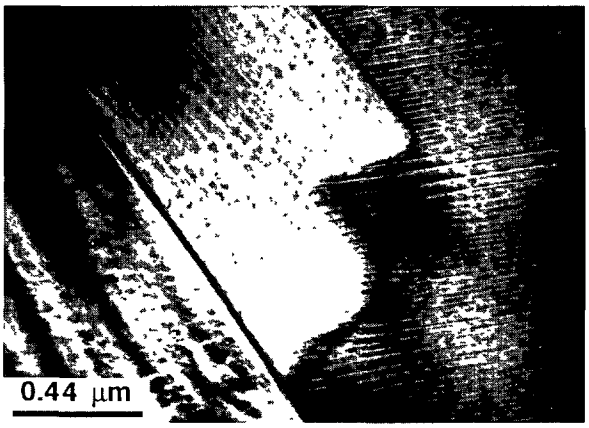

Fig. 1. — Bright field electron micrograph Domain microstructure in $Mn_{2\,61}Fe_{0\,39}O_4$ – Laths internally twinned.

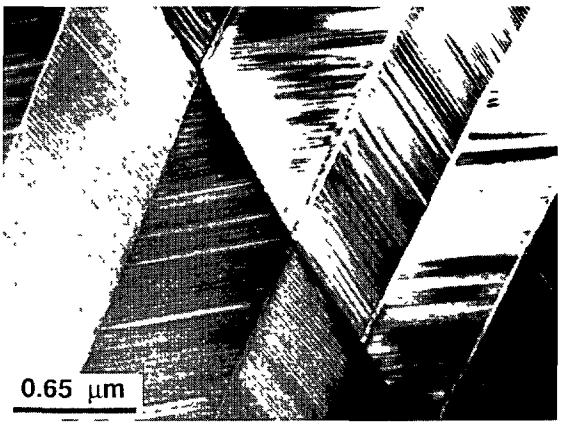

Fig 2 — Bright field electron micrograph. Domain microstructure in $Mn_{2\,42}Fe_{0\,58}O_4$ – Laths internally twinned.

$x \geq 1.05$. Moreover, TEM results show that, as long as the samples have a tetragonal crystal line structure, a domain microstructure is observed.

• $x = 0.39$ (Fig. 1): TEM reveals laths of about 0.5–1 μm wide; each of them is internally twinned, with the twins being about 5–20 nm wide. The domain walls are parallel to the {101} planes of the cubic cell.

• $x = 0.58$ (Fig. 2): A domain structure is as well observed. The lath width ranges from 0.4 to 0.8 μm, and the internal twins are still present and well marked (10–20 nm wide).

• $x = 0.78$ (Fig. 3): The lath width clearly decreases (50–100 nm), and the internal twins inside each lath are hardly visible (about 5 nm wide). So, as soon as the tetragonality of the sample decreases, the lath width also decreases and the internal twinning (lamellae) tends to vanish. All the twin walls are parallel to {101}.

• $x = 1.05$ (Fig. 4): For this x value, a special microstructure is observed, the sample being relatively heterogeneous. Fine striations are observed parallel to ⟨110⟩ space at a range

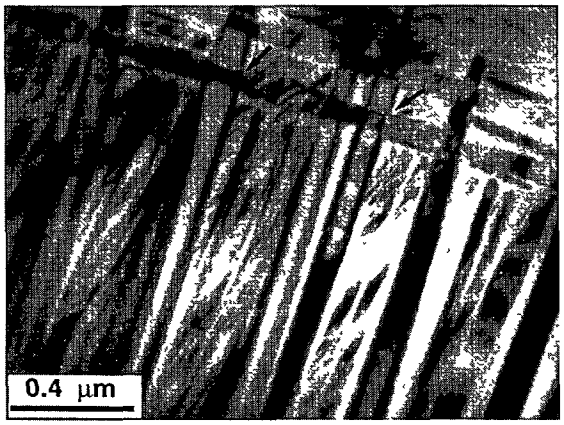

Fig. 3. — Bright field electron micrograph. Domain microstructure in $Mn_{2.22}Fe_{0.78}O_4$ – Two sets of nearly perpendicular domains. Note the wall interactions at crossing (arrow).

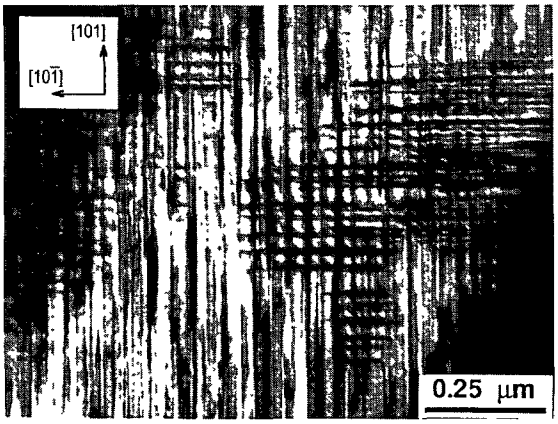

Fig. 4. — Bright field electron micrograph. "Tweed" microstructure in $Mn_{1.95}Fe_{1.05}O_4$.

from a few nanometers to 40 nm. In those areas where the striations are more dense, this microstructure is very similar to the "tweed structure" already reported by the authors in Ni and Co manganites [9].

• $x > 1.05$ (Figs. 6 and 7) Grains free of two-dimensional defects are now observed. Note that for $x = 1.30$, dislocation pile-ups are frequently observed forming low-angle boundaries (Fig. 6). These dislocations have the well-known Burgers vector of the spinel structure $b = \frac{1}{2}\langle 110\rangle$ [16], generally dissociated into two colinear partials $b = \frac{1}{4}\langle 110\rangle$. The dissociation width is about 5–6 nm.

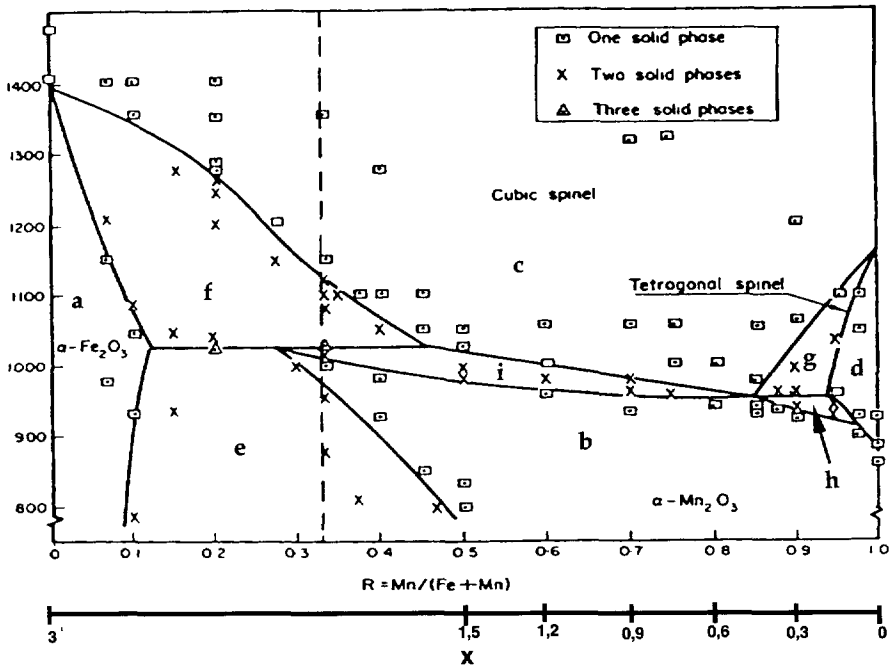

(a) $\alpha-Fe_2O_3$ (structure corundum)
(b) $\alpha-Mn_2O_3$ (C-rare-earth oxide structure)
(c) cubic spinel
(d) tetragonal spinel
(e) $\alpha-Fe_2O_3 + \alpha-Mn_2O_3$
(f) $\alpha-Fe_2O_3$ + cubic spinel
(g) cubic spinel + tetragonal spinel
(h) $\alpha-Mn_2O_3$ + tetragonal spinel
(i) $\alpha-Mn_2O_3$ + cubic spinel

Fig 5. — Equilibrium diagram of the system $Fe_3O_4-Mn_3O_4$ [15].

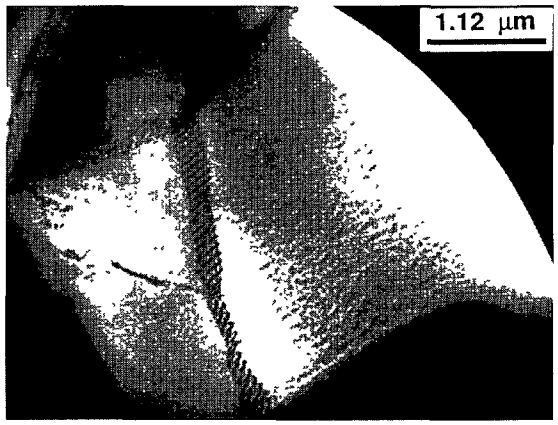

Fig. 6. — Bright field electron micrograph. Low angle boundary in $Mn_{1.70}Fe_{1.30}O_4$. No two-dimensional defects are observed

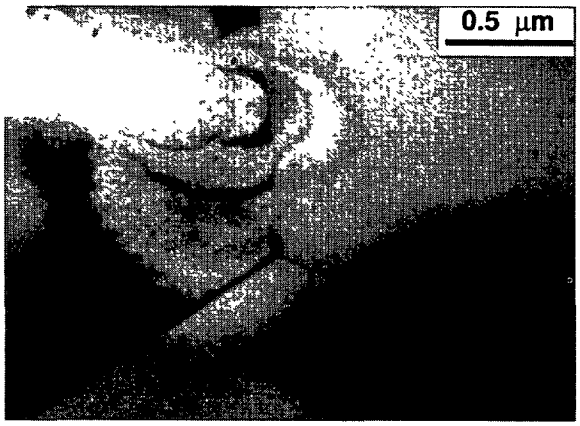

Fig. 7. — Bright field electron micrograph. These grains ($Mn_{1\ 49}Fe_{1\ 51}O_4$) are free of two-dimensional defects.

Table V. — *Iron manganite ceramics before ageing* ($t = 0$)*: cationic distributions computed from Mössbauer data.*

Iron content, x	Cationic distributions
0.39	$Mn^{2+}_{0\ 78}Fe^{3+}_{0.22}[Fe^{3+}_{0.17}Mn^{3+}_{1\ 61}Mn^{2+}_{0.22}]O^{2-}_4$
0.58	$Mn^{2+}_{0\ 71}Fe^{3+}_{0\ 29}[Fe^{3+}_{0\ 29}Mn^{3+}_{1.42}Mn^{2+}_{0\ 29}]O^{2-}_4$
0.78	$Mn^{2+}_{0\ 71}Fe^{3+}_{0\ 29}[Fe^{3+}_{0\ 49}Mn^{3+}_{1\ 22}Mn^{2+}_{0.29}]O^{2-}_4$
1.05	$Mn^{2+}_{0\ 77}Fe^{3+}_{0\ 23}[Fe^{3+}_{0\ 82}Mn^{3+}_{0\ 95}Mn^{2+}_{0\ 23}]O^{2-}_4$
1.30	$Mn^{2+}_{0\ 73}Fe^{3+}_{0\ 27}[Fe^{3+}_{1\ 03}Mn^{3+}_{0\ 70}Mn^{2+}_{0.27}]O^{2-}_4$
1.51	$Mn^{2+}_{0\ 70}Fe^{3+}_{0\ 30}[Fe^{3+}_{1\ 21}Mn^{3+}_{0\ 49}Mn^{2+}_{0\ 30}]O^{2-}_4$

4. Discussion

4.1. Electrical Properties. — The cationic distributions given by $Mn^{2+}_{1-y}Fe^{3+}_y[Fe^{3+}_z Mn^{3+}_{2-x}Mn^{2+}_y]O^{2-}_4$ with $x = y + z$ [11] can be inferred by correlation of the results obtained by XRD, Mössbauer spectroscopy and electrical measurements. Table V recalls the cationic distributions of iron manganite for $0.39 \leq x \leq 1.51$ before ageing ($t = 0$). Moreover, the origin of the ageing observed on iron manganite thermistors has been identified in a previous work [12]. This is related to the migration of Fe^{3+} ions in octahedral sites. The number of Fe^{3+} ions in tetrahedral sites is nearly constant (see Tab. V), so we can assume that, as x increases, the number of Fe^{3+} ions, which migrate toward octahedral sites, remains constant. Thus the number of Fe^{3+} ions remaining in A sites after 1000 hours ageing is constant and equal to 0.08, as indicated by the Mössbauer results for two values of x (0.58 and 1.05) in Table IV. On light of this assumption, Table VI reports the cationic distributions obtained for different iron contents in iron manganites after 1000 hours ageing ($t_{1000\ h}$).

According to the cationic distributions proposed for iron manganites before and after ageing (Tabs. V and VI), both Mn^{2+} and Mn^{3+} are present in B sites so that the conditions are correct for electron hopping from Mn^{2+} and Mn^{3+} [17]. The conductivity of the material is determined by the number of ions capable of either donating or accepting electrons in this

Table VI. — *Iron manganite ceramics after ageing* ($t = 1000$ *h*)*: cationic distributions computed from Mössbauer data.*

Iron content, x	Cationic distributions
0.39	$Mn^{2+}_{0\ 92}Fe^{3+}_{0.08}[Fe^{3+}_{0\ 31}Mn^{3+}_{1\ 61}Mn^{2+}_{0.08}]O^{2-}_4$
0.58	$Mn^{2+}_{0\ 92}Fe^{3+}_{0\ 08}[Fe^{3+}_{0\ 50}Mn^{3+}_{1\ 42}Mn^{2+}_{0\ 08}]O^{2-}_4$
0.78	$Mn^{2+}_{0\ 92}Fe^{3+}_{0\ 08}[Fe^{3+}_{0\ 70}Mn^{3+}_{1\ 22}Mn^{2+}_{0\ 08}]O^{2-}_4$
1.05	$Mn^{2+}_{0\ 92}Fe^{3+}_{0\ 08}[Fe^{3+}_{0\ 97}Mn^{3+}_{0\ 95}Mn^{2+}_{0\ 08}]O^{2-}_4$
1.30	$Mn^{2+}_{0\ 92}Fe^{3+}_{0\ 08}[Fe^{3+}_{1\ 22}Mn^{3+}_{0\ 70}Mn^{2+}_{0\ 08}]O^{2-}_4$
1.51	$Mn^{2+}_{0.92}Fe^{3+}_{0\ 08}[Fe^{3+}_{1\ 43}Mn^{3+}_{0\ 49}Mn^{2+}_{0\ 08}]O^{2-}_4$

Table VII. — *Probability* $C(1-C)$ *of iron manganite thermistors before* ($t = 0$) *and after ageing* ($t = 1000$ *h*) *and* $\Delta[C(1-C)]$*, i.e. is the variation of the probability* $C(1-C)$ *between* $t = 0$ *and* $t = 1000$ *h.*

Iron content, x	0.39	0.58	0.78	1.05	1.30	1.51
$C(1-C)_{t=0}$	0.110	0.141	0.155	0.167	0.207	0.235
$C(1-C)_{t=1000\ \mathrm{h}}$	0.045	0.050	0.058	0.071	0.092	0.120
$\Delta[C(1-C)]$	0.065	0.091	0.097	0.096	0.115	0.115

electron transfer. Thus the electrical conductivity can be written:

$$\sigma = \frac{\sigma_0}{T} NC(1-C)\exp\left(\frac{-E_H}{kT}\right) \quad \text{with} \quad \sigma_0 = \frac{N_{oct}e^2d^2\nu_0}{k}$$

where N_{oct} is a concentration per cm^3 of octahedral sites, d is a jump distance for the charge carrier, ν_0 is the lattice vibrational frequency associated with conduction, k is Boltzmann's constant, e the electronic charge, N is a concentration per formulae unit of sites which are available to the charge carriers, C is a fraction of available sites which are occupied by the charge carriers, and E_H is a hopping energy. The term $C(1-C)$ can be rewritten:

$$C(1-C) = \frac{(Mn^{3+}_{oct})(Mn^{2+}_{oct})}{[(Mn^{3+}_{oct}) + (Mn^{2+}_{oct})]^2}$$

which represents the probability of finding Mn^{3+} Mn^{2+} pairs in octahedral sites.

Table VII indicates the probability $C(1-C)$ of iron manganite thermistors before and after ageing and also $\Delta[C(1-C)]$, which represents the variation in the probability C(1-C) between $t = 0$ and $t = 1000$ h. This variation increases with the iron content; this correlation shows that the relative *variation* in conductivity (or resistivity *i.e.* $\Delta R/R$) between $t = 0$ and $t = 1000$ h increases with the iron content, Table II. This result may explain the increase in ageing after 1000 h with the increase of iron content (see Fig. 8).

4.2. XRD AND TEM OBSERVATIONS. — As is clear from the equilibrium diagram (Fig. 5), since the quenching temperature is 1180 °C, all samples should crystallize in the cubic spinel phase. Or, for $x < 1.05$, our samples crystallize in quadratic spinel phase. This discrepancy could be explained by the difference between the methods of ceramics preparation (soft chemistry or conventional method) or by an imperfect air quenching.

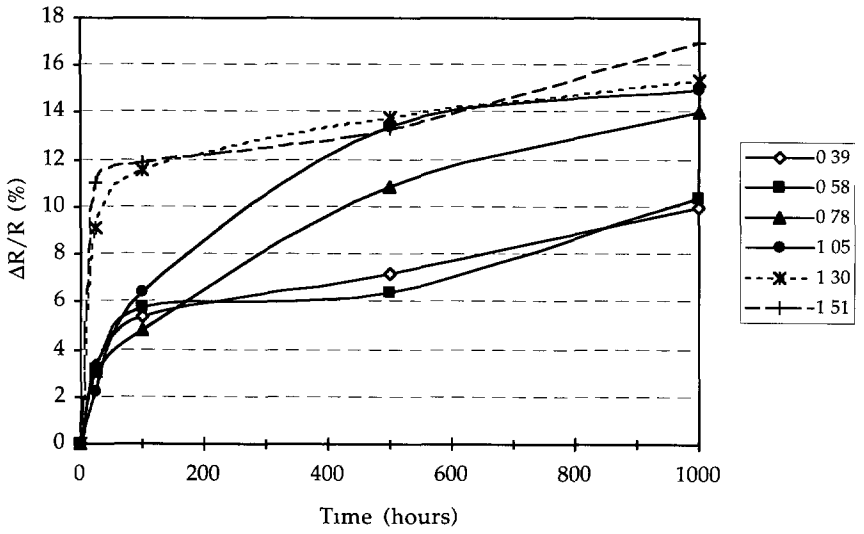

Fig. 8. — Variation of $\Delta R/R$ as a function of ageing time.

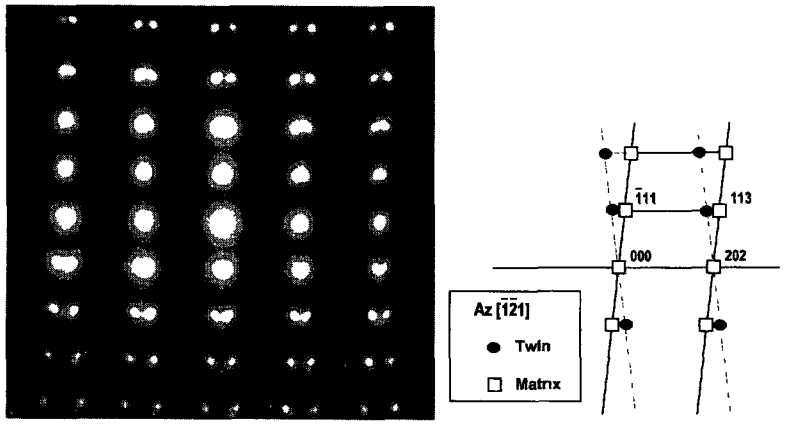

Fig. 9. — Electron diffraction pattern of a lath Az[121]. The row of unsplit spots is normal to the twin interface (101).

4.2.1. $x < 1.05$. — The presence of a low temperature stable tetragonal crystal structure suggests that the air quenching was imperfect and did not allow the cubic spinel to stabilize, so a cubic-to-tetragonal transition occurred during cooling. A similar transformation, due to the cooperative Jahn-Teller effect, has been studied in detail by the authors in Mn_3O_4 hausmannite [16]: transformation twinning results from this structural transition, which promotes the formation of domains (orientation states). These are created in the low symmetry phase, having the same structure but different orientations, and occur to relieve the long-range stresses created by the transition (accommodation twins).

According to Aizu's definition [18], this transition may be ferroelastic, as it is in hausmannite, since the point group of low-symmetry phase (4/mmm) is a subgroup of the "prototypic" cubic phase (m3m). We have also shown in [14] that, in such accommodation twins, the lath walls

Table VIII. — *Compositions of the cubic-quadratic transition in $Mn_{3-x}Fe_xO_4$ spinels for different authors.*

Authors	Compositions
Holba *et al.* [21]	Mn_2FeO_4
Ishii *et al.* [22]	$Mn_{2\ 25}Fe_{0\ 75}O_4$
Brabers [23]	$Mn_{1\ 9}Fe_{1\ 1}O_4$
Cervinka *et al.* [24]	$Mn_{1\ 9}Fe_{1\ 1}O_4$
Wickham [15]	Mn_2FeO_4

form incoherent boundaries, whereas the lamellae walls of the internal twins are coherent twin boundaries. Indeed an electron diffraction pattern of a lath (Fig. 9) shows a row of unsplit spots perpendicular to the twinning plane {101}, characteristic of a type -I mechanical twin: the twin and its matrix are related by a reflection across the twin plane. The orientation of the domain walls, parallel to {101} planes, is in agreement with theoretical predictions [19].

In Figure 3, orthogonal domains cross each other, and a sharp deformation of the walls is clearly visible. These interactions, which were investigated in detail in [20], are characteristic of ferroelastic domains.

4.2.2. $x = 1.05$. — For this value, that is near the cubic-tetragonal transition limit for our samples and for other authors (Tab. VIII), we observe the "tweed structure"; this structure may be interpreted in two ways. First, it may result from a very dense microtwinning in {101} planes. Secondly, it might result from the decomposition of the solid solution during cooling. In the present case, it is possible that these fine lamellae are alternatively Mn rich and Fe rich.

4.2.3. $x > 1.05$. — No phase transition is possible during cooling and, accordingly, the microstructure is formed with cubic spinel grains free from planar defects. The dislocation pile-up observed is probably related to the thermal processing of the sample: during the air cooling, a recovery occurs that leads to a reorganization of the as-grown dislocations. As mentioned above, the dislocations present in the spinel cubic phase are split and the dissociation width is great enough to be easily observed by TEM. On the other hand, in hausmannite Mn_3O_4, dissociation of perfect dislocations was not detected, even using weak-beam dark field imaging, which indicates that the dissociation distance was probably less than 2–3 nm. It can be concluded that the addition of iron markedly lowers the fault energy.

Our TEM observations are in good agreement with those reported in [25] on iron manganites $Mn_{3-x}Fe_xO_4$ with $x = 1$, 1.05 and 1.30. For $x = 1$, similar domains were observed limited by {101} planes, whereas for $x = 1.05$, a tweed structure was revealed. For $x = 1.30$, no planar defects were observed. The domain structure was also explained as the result of a cubic-to-tetragonal transition.

4.3. Correlation Between Microstructure and Ageing. — The TEM observations correlated with the electrical measurements show that the microstructure has a non-negligible effect on electrical properties. In previous papers, we have shown that the existence of planar defects is related to an improvement of the electrical stability [9, 26]. Since ageing is believed to be correlated to the atomic diffusion in a spinel lattice, these defects could act as barriers against ion mobility, thus explaining the better electrical stability of ceramics having defects. Moreover, we have shown that the origin of the ageing in iron manganite is correlated to the

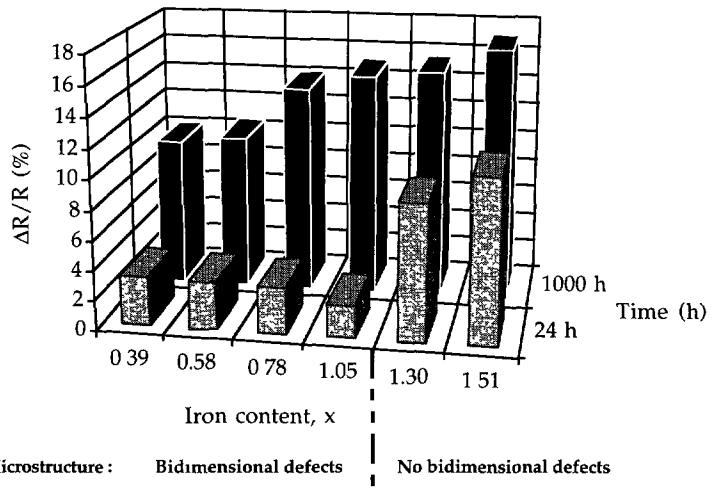

Fig 10. — Variation of ageing at 24 and 1000 hours as a function of iron content and microstructure.

migration of Fe^{3+} and Mn^{2+} ions between the A and B sublattices of spinel structure. Does the microstructure of solid-solution $Mn_{3-x}Fe_xO_4$ have any effect on electrical properties?

From Figure 10, it is clear that the ageing after 1000 hours is correlated with the microstructure. For $x = 0.39$ and $x = 0.58$, TEM reveals large laths and internal twins, and the ageing is about 10%. For $x = 0.78$, the lath width clearly decreases and ageing ($t = 1000$ h) increases to 14%. For $x = 1.05$, a value close to the limit between the tetragonal and cubic phases, the domain structure disappears and TEM reveals a tweed microstructure, as the ageing increases about 15%. Lastly, when grains free of two-dimensional defects are observed, the ageing reaches about 17%. Unambiguously, the presence of planar defects hampers ion migration and consequently prevents the increase of $\Delta R/R$. The phenomenon is enhanced at 24 hours of ageing. From Figure 10, it is clear that, as soon as the sample has the tetragonal structure with a more or less pronounced domain structure, the variation of resistance between $t = 0$ and $t = 24$ hours is very low, $\Delta R/R$ is about 3% (high density of planar defects); $\Delta R/R$ increases abruptly for $x = 1.30$ ($\Delta R/R = 9,1\%$) and reaches about 11% with no defects. So the presence of defects does play a role in the kinetics of ion migration: it slows down the ion migration at the beginning of the ageing.

5. Conclusion

Previously, we have shown that the origin of ageing of iron manganite thermistors is due to the migration of Fe^{3+} and Mn^{2+} ions between tetrahedral and octahedral sites of the spinel structure. In this paper, the electrical measurements show that the ageing depends on the composition, as it increases with the iron content. TEM observations reveal two-dimensional defects for $x \leq 1.05$ and no planar defects are detected for $x > 1.05$.

The correlation between the microstructure and the ageing indicates that the presence of these defects hampers ion migration. Consequently:

i) the ageing kinetic is slowed down by the existence of defects;

ii) defects stabilize the electrical properties.

References

[1] Macklen E.D., Thermistors (Electrochem. Publ. Ayr. Scotland, 1979).

[2] Jabry E., Boissier G., Rousset A., Carnet R. and Lagrange A., Preparation of semiconducting NTC Thermistors by Chemical Method., *J. Phys. Colloq. France* **47** (1986) C1-843-847.

[3] Feltz A., Töpfer J. and Schirrmeister F., Conductivity data and preparation routes for $NiMn_2O_4$ thermistor ceramics, *J. Eur. Ceram. Soc.* **9** (1992) 187-191.

[4] Macklen E.D., Electrical conductivity and cation distribution in nickel manganite, *J. Phys. Chem. Solids* **47** (1986) 1073-1079.

[5] Metz R., Caffin J.P., Legros R. and Rousset A., The preparation, characterization and electrical properties of copper manganites $Cu_xMn_{3-x}O_4$, $(0 < x < 1)$, *J. Mater. Sci.* **24** (1989) 83-87.

[6] Vervey E.J.M., Haaij P.W., Romeijn F.C. and Van Oosternout C.W., Controlled-valency semiconductors, *Philips Res. Rep.* **5** (1950) 173-187.

[7] Caffin J.P., Thesis, University Paul Sabatier (Toulouse, France, 1986).

[8] Metz R., Thesis, University Paul Sabatier (Toulouse, France, 1991).

[9] Brieu M., Couderc J.J., Rousset A. and Legros R., TEM Characterization of nickel and nickel-cobalt manganite ceramics, *J. Eur. Ceram. Soc.* **11** (1993) 171-177.

[10] Fritsch S., Thesis, University Paul Sabatier (Toulouse, France, 1995).

[11] Battault T., Legros R. and Rousset A., Structural and electrical properties of iron manganite spinels in relation with cationic distribution., *J. Eur. Ceram. Soc.* **15** (1995) 1141-1147.

[12] Battault T., Thesis, University Paul Sabatier (Toulouse, France, 1995).

[13] Gillot B., Laarj M., Kacim S., Battault T., Legros R. and Rousset A., Cationic distribution and oxidation kinetics of divalent manganese ions in iron manganite spinels $Mn_{3-x}Fe_xO_4$ $(0 < x < 1.50)$, *Solid State Ionics* **83** (1996) 215-263.

[14] Singh V.K., Khatri N.K. and Lokanathan S., Mössbauer study of $Co_xMn_{3-x-y}Fe_yO_4$ and $Ni_xMn_{3-x-y}Fe_yO_4$ systems, *Ind. J. Pure & Appl. Phys.* **20** (1982) 83-89.

[15] Wickham D.G., The Chemical Composition of Spinels in the System Fe_3O_4–Mn_3O_4, *J. Inorg. Nucl. Chem.* **31** (1969) 313-320.

[16] Couderc J.J., Fritsch S., Brieu M., Vanderschaeve G., Fagot M. and Rousset A., A Transmission Electron Microscopy Study of Lattice Defects in Mn_3O_4 Hausmannite, *Philos. Mag. B* **70** (1994) 1077-1094.

[17] Dorris S.E. and Mason T.O., Electrical properties and cations valencies in Mn_3O_4, *J. American Ceramic Society* **71** (1988) 379-385.

[18] Aizu K., Possible Species of Ferromagnetic, Ferroelectric and Ferroelastic Crystals, *Phys. Rev. B* **2** (1970) 754-772.

[19] Sapriel J., Domain-wall Orientations in Ferroelastics, *Phys. Rev. B* **12** (1975) 5128-5140.

[20] Snoeck E., Casanove M.J., Baules P. and Roucaud C., Ferroelastic behaviour of the $(Ln)Ba_2Cu_3O_{6+x}$ Orthorhombic Phase, *Ferroelectrics* **97** (1989) 181-186.

[21] Holba P., Khilla M.A. and Krupicka S., On the Miscibility Gap of Spinels $Mn_xFe_{3-x}O_{4+\gamma}$, *J. Phys. Chem. Solids* **34** (1973) 387-395.

[22] Ishii M., Nakahira M. and Yamanaka T., Infrared absorption spectra and cation distribution in $(Mn, Fe)_3O_4$, *Solid State Communications* **11** (1972) 209-212.

[23] Brabers V.A.M., Cation Migration, Cation Valencies and the Cubic-Tetragonal Transition in $Mn_xFe_{3-x}O_4$, *J. Phys. Chem. Solids* **32** (1971) 2181-2191.

[24] Cervinka L., Hosemann R. and Vogel W., Paracrystalline lattice distorsions and microdomains in manganese ferrites near the cubic to tetragonal transition, *Acta Cryst. A* **26** (1970) 277-289.

[25] Van Landuyt J., De Ridder R., Brabers V.A M. and Amelinckx S , Jahn-Teller Domains in $Mn_xFe_{3-x}O_4$ as observed by Electron Microscopy, *Mat. Res. Bull.* **7** (1972) 327-338.

[26] Rousset A., Lagrange A., Brieu M., Couderc J.J. et Legros R., Influence de la microstructure sur la stabilité électrique des thermistances CTN, *J. Phys. III France* **3** (1993) 833-845.